J Mol Model (2013) 19:3245–3253
DOI 10.1007/s00894-013-1828-6

ORIGINAL PAPER

Degradation of polyvinyl alcohol under mechanothermal stretching

Dahiyana Cristancho · Yan Zhou · Rodrigo Cooper · David Huitink · Funda Aksoy · Zhi Liu · Hong Liang · Jorge M. Seminario

Received: 18 December 2012 / Accepted: 19 March 2013 / Published online: 7 May 2013

Abstract Mechanical and thermal properties of polyvinyl alcohol (PVA) are characterized and analyzed using in situ X-ray photoelectron spectroscopy (XPS) and quantum chemistry calculations. It is found that the carbon peaks—commonly used as the reference for spectroscopic analysis—shift under mechanical and thermal stretching. Results also indicate that, at different temperatures and among the various functional groups present in PVA, the carbon in the C–O group is the most stable. Computational calculations showed that Hartree–Fock/10-31G (d) reproduces the binding energy of core carbon electrons with an accuracy of 95 %, which is enough to characterize bonds, allowing the results of the spectroscopic analysis to be corroborated.

Dahiyana Cristancho and Yan Zhou contributed equally to this research.

D. Cristancho · J. M. Seminario (✉)
Department of Chemical Engineering, Texas A&M University, College Station, TX, USA
e-mail: seminario@tamu.edu

D. Cristancho · Y. Zhou · H. Liang (✉) · J. M. Seminario
Materials Science and Engineering Graduate Program, Texas A&M University, College Station, TX, USA
e-mail: hliang@tamu.edu

Y. Zhou · R. Cooper · D. Huitink · H. Liang
Department of Mechanical Engineering, Texas A&M University, College Station, TX, USA

J. M. Seminario
Department of Electrical and Computer Engineering, Texas A&M University, College Station, TX, USA

F. Aksoy · Z. Liu
Advanced Light Source, Lawrence Berkeley National Laboratory, Berkeley, CA, USA

Keywords XPS · PVA · Binding energy · Deconvolution · Quantum chemistry · *Ab initio*

Introduction

Mechanical forces have significant effects on the behavior of materials; they can induce the oxidation of metals [1–8] and alter the pathways of electrons in an organic molecule [9]. Understanding the mechanisms of mechanoactivated chemical reactions is the key to obtaining control over and precise predictions of materials. Besides mechanical activation, thermal energy also affects the behavior of materials such as polymers [10]. Polyvinyl alcohol (PVA) is one of the most-studied polymers in the chemical industry, as well as in experimental and computational research laboratories. PVA has an extensive range of applications in, for example, adhesives [11], textile sizing [12], surfactants [13], and membranes for sound absorption [14]. The chemical structure of PVA consists of a carbon backbone with hydroxyl groups along the chain (Fig. 1b). PVA is soluble in water and interacts with other molecules through hydrogen bonding, crosslinking, and oxidation. Mechanical properties of polymers, such as their resistance to stress cracking and fluid resistance, can be improved using crosslinking reactions. Crosslinked polymers are used in medical implants because of their low cytotoxicity and high biocompatibility [15]. They can be made through exposure to radiation, such as an electron beam [16], gamma radiation [17], or X-ray radiation [18].

Akhter *et al.* reported the first X-ray photoelectron spectroscopic (XPS) analysis of PVA. Three degradation routes were found: crosslinking to form an ether group, oxidation to form a carbonyl group, and oxidative-induced chain scission to form a carboxylated group [19]. Beamson *et al.* reported that the

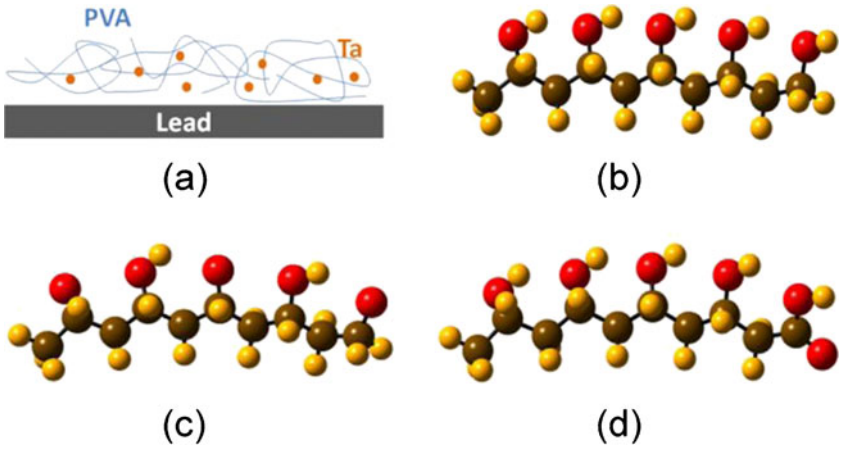

Fig. 1 **a** Cartoon of a PVA-Ta-Pb sheet. **b** Optimized structure of polyvinyl alcohol (PVA), $C_{10}H_{22}O_5$. **c** Optimized structure of PVA with ketone groups RC(=O)R, $C_{10}H_{19}O_5$. **d** Carboxyl group C–O at the end of the chain, $C_{10}H_{20}O_5$. C atoms are shown in *brown*, O in *red*, and H in *yellow*

initial rate of degradation of PVA varied linearly with X-ray intensity. The C–O functional groups are broken during PVA degradation, creating a blend of polymers with functionalities such as CH_2–CO_2R_1, CH_2, C=O, and CO_2R_2 [20].

The molecular orbital energies of core electrons correspond to the binding energies obtained from XPS. When a sample surface is irradiated with X-rays, the core electrons are ejected if enough energy is provided to ionize their atoms. Thus, the molecular orbital energies can be obtained experimentally and theoretically. In the analysis of XPS spectra, the carbon peaks are commonly used as references for calibration. However, the reliability of such references is an issue when the samples are mechanothermally stretched.

In the work described in the present paper, we investigated the chemistry of PVA that is coated onto a lead sheet with dispersed tantalum powder (Fig. 1a). When heated in situ, the PVA expanded with the help of the mechanical stretching provided by the lead. Both high and low molecular weight PVA were characterized using XPS. The binding energies of several carbon species were analyzed using first-principles quantum chemistry. Among the various functional groups present in PVA, the carbon in the C–O group was found to be the most stable at different temperatures. All of the binding energies for standard carbon peaks were reproduced with an accuracy of 95 %.

Experimental section

Materials Lead sheet (McMaster-Carr, Atlanta, GA, USA) was cold-rolled unidirectionally to achieve a thickness of 0.35 mm and cleaned with acetone before use. Polydisperse polyvinyl alcohol (PVA) of molecular weight (MW) 10,000 g/mol (PVA-10 k) and 150,000 g/mol (PVA-150 k) was purchased from Sigma–Aldrich (St. Louis, MO, USA). Tantalum powder (60–100 mesh, Sigma–Aldrich) was used as received.

PVA-Ta-Pb sample preparation and XPS measurement Ta powder was mixed with a solution of PVA containing DI water at a concentration of 50 wt.%. The mixture was coated onto the cold-rolled lead sheet using a single-wafer spin processor (Laureli Technologies Corp., North Wales, PA, USA) at 600 rpm and later left to dry in air at 23 °C. Samples were tested at the Advanced Light Source via ambient-pressure X-ray photoelectron spectroscopy (AP-XPS), performed using beamline 9.3.2 [21]. The samples were sputtered with Ar^+ (10^{-5} Torr) at 1.5 keV for 20 min prior to data acquisition. A sample holder equipped with a ceramic-coated button heater and a K-type thermocouple was used to monitor the temperature of the sample in an ultrahigh vacuum (UHV) chamber. The sample was scanned with 550-eV X-rays as its temperature was elevated from 310 K to 345 K by the heater. Using the software package CasaXPS version 2.3.14, the C (1*s*) peaks were deconvoluted using asymmetric Gaussian–Lorentzian line shapes with a Shirley background. The deconvoluted carbon peaks were constrained to have equal full widths at their half-maxima (i.e., equal FWHMs). The residual standard deviation (STD) was minimized during each deconvolution process.

Computational section 5-mer polyvinyl alcohols with the molecular structures $C_{10}H_{22}O_5$, $C_{10}H_{19}O_5$ and $C_{10}H_{20}O_6$ (Fig. 1b, c, d) were optimized until local minima were obtained. A second-derivative calculation was performed for each optimized structure to check that the optimized geometries corresponded to local minima. The carbon–carbon bond lengths were then elongated by 5 % (to mimic the bond stretching produced by changes in temperature) while all other coordinates were constrained, and the geometries were re-optimized, leading to a structure called PVA-5. In order to validate the experimental data obtained from XPS analysis, we used the DFT B3PW91 hybrid functional, which includes the Becke-3 exchange functional [22] and the Perdew–Wang 91 correlation functional [23, 24] as well as the Hartree–Fock (HF) method. All calculations were performed using the

Gaussian 09 program [25]. The basis sets used were STO-nG (n=3 and 6) [26–28], 6-31G(d) [29, 30], 3-21G(d) [31–35], and cc-pVDZ [36], which were employed to reproduce the values for the C(1S) binding energy (BE). A large amount of data highlighting the importance of DFT and HF methods as well as the modeling of several experiments have been published; see for instance [37–51] and references therein.

Results and discussion

The experimental results showed that the binding energy (BE) of PVA is dependent on its molecular weight. Figure 2 shows the XPS spectra of PVA-10 k and PVA-150 k. The BEs of the major carbon peaks are around 285 eV, which matches the values reported in the literature [19, 52–54]. For the major peaks in PVA-10 k, there is a 0.2-eV increase in the BE when the temperature is changed from 310 K to 345 K; the increase is larger (0.9 eV) for PVA-150 k. This increase in BE may be considered a signature of polymer degradation through oxidation. Once the chemical bond (C–O) is formed, the changes in the valence electron charge yield an increase in BE.

The carbon species in PVA-10 k and PVA-150 k were determined by the deconvolution process. As shown in Fig. 3, four functional groups are found at the low temperature for PVA-10 k and PVA-150 k: saturated hydrocarbon groups (C–H) at 284.6 eV and 283.8 eV, alcohol groups (C–O) at 285.6 eV and 285.2 eV, carbonyl groups (C=O) at 287.0 and 286.5 eV, and carboxylate groups (O–C=O) at 289.5 eV and 288.8 eV. The presence of O–C=O and C=O shows that the PVA samples are damaged by the sputtering process.

Degradation mechanism

Thermal evolution results (Fig. 4) suggest that PVA chemically degrades at 308–345 K. PVA-10 k and PVA-150 k have different thermal degradation mechanisms (Fig. 5). When the temperature of PVA-10 k is raised from 310 K to 345 K (Fig. 4a), the concentration of C–C increases at the same rate that the concentration of C–O decreases, leaving the C=O and O–C=O groups practically unchanged. This behavior may be attributed to the X-ray irradiation of a low molecular weight polymer. The irradiation breaks C–O bonds, leading to unbound C that is ready to bind to the nearest C (polymerization by entanglement), generating hydrogen peroxide as the by-product (Fig. 5a). Different behavior is observed for PVA-150. When the temperature is raised from 308 K to 345 K, the concentration of C–C decreases (depolymerization) at the same rate that the concentration of C–O (crosslinked degradation/oxidation) increases (Fig. 4a); however, the concentration of C=O remains constant. There is also another signature of oxidation: the concentration of O–C=O species decreases when the C–O or C=O bond breaks, allowing the formation of C–O–C. This behavior suggests that a crosslinking

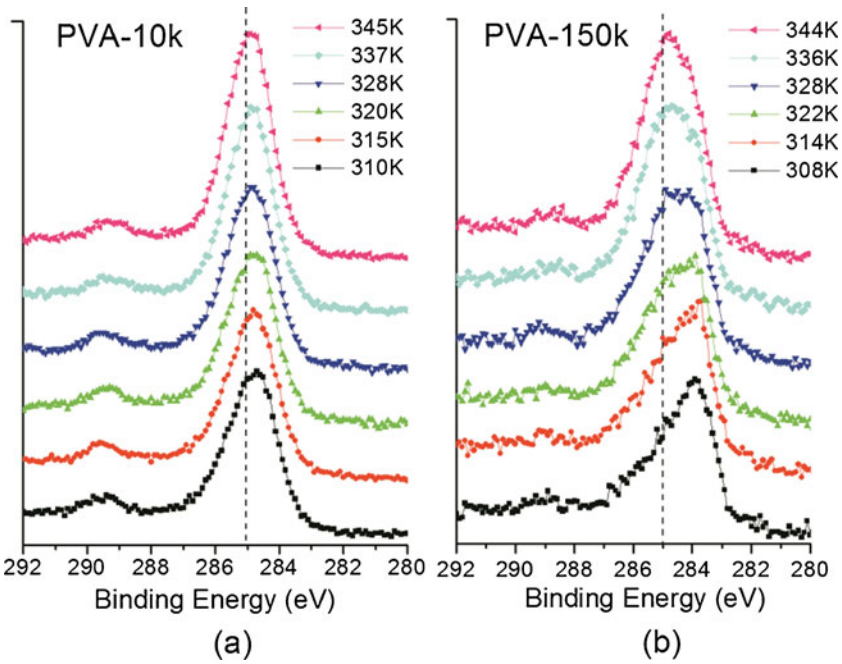

Fig. 2a–b The XPS spectra of PVA-10 k and PVA-150 k as a function of temperature from 310 K to 345 K (PVA-10 k) and from 308 K to 344 K (PVA-150 k). **a** PVA-10 k; **b** PVA-150 k

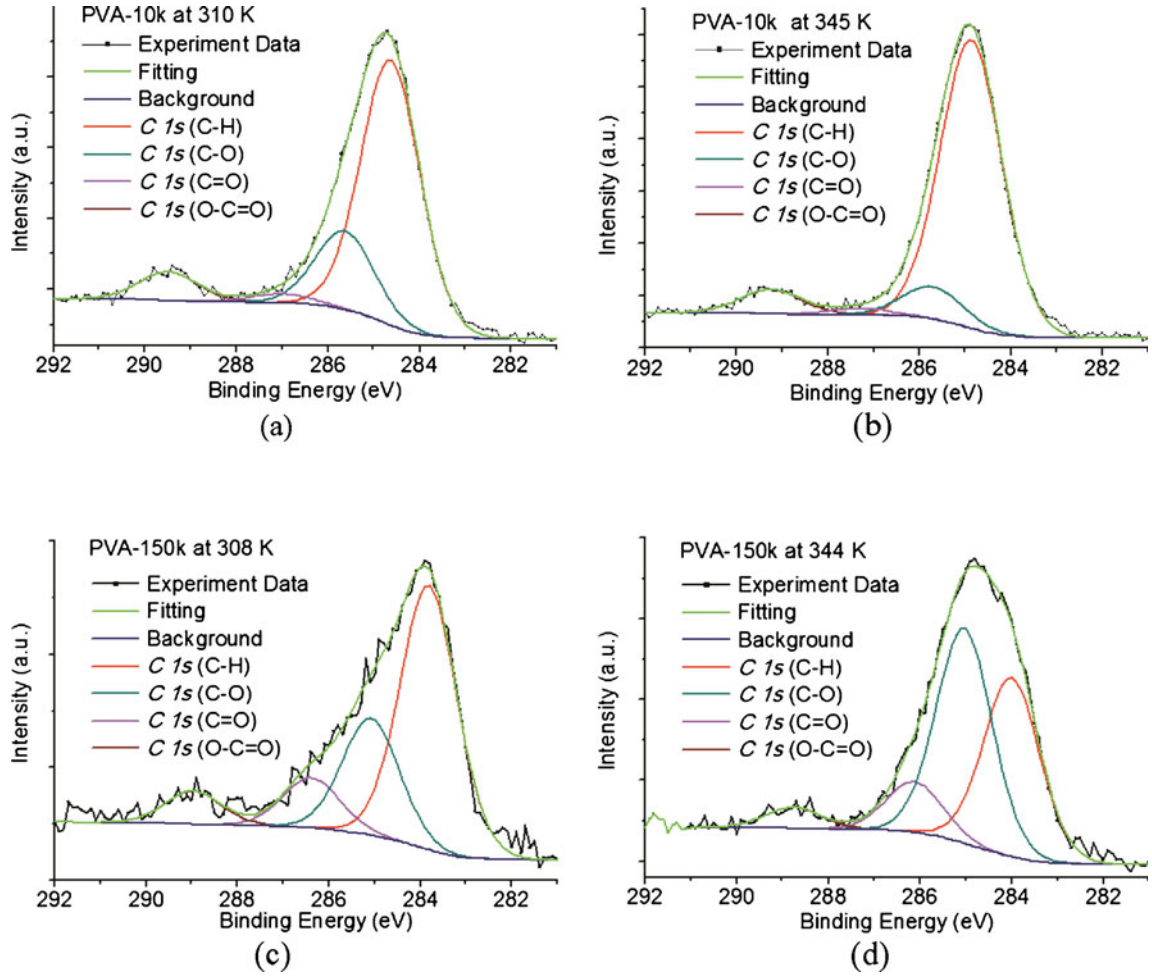

Fig. 3a–d Deconvoluted C (1*s*) spectra of saturated hydrocarbon groups (C–H), alcohol groups (C–O), carbonyl groups (C=O), and carboxylate groups (O–C=O). **a** PVA-10 k at 310 K; **b** PVA-10 k at 345 K; **c** PVA-150 k at 308 K; **d** PVA-150 k at 344 K

reaction may take place once the temperature is raised, liberating H_2O as by-product of the reaction (Fig. 5b). The resulting carbon species has the same BE and was reported elsewhere [20].

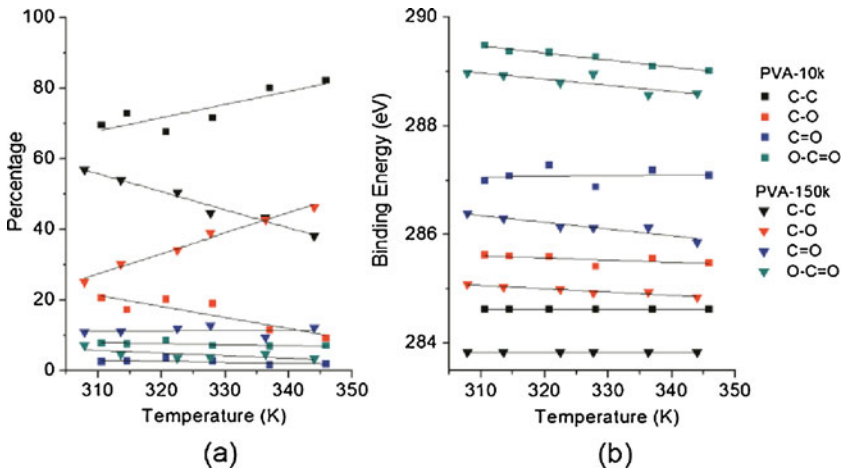

Fig. 4a–b Functional group compositions (**a**) of PVA species versus temperature, as well as the corresponding BEs of these groups (**b**) calibrated with respect to C–C

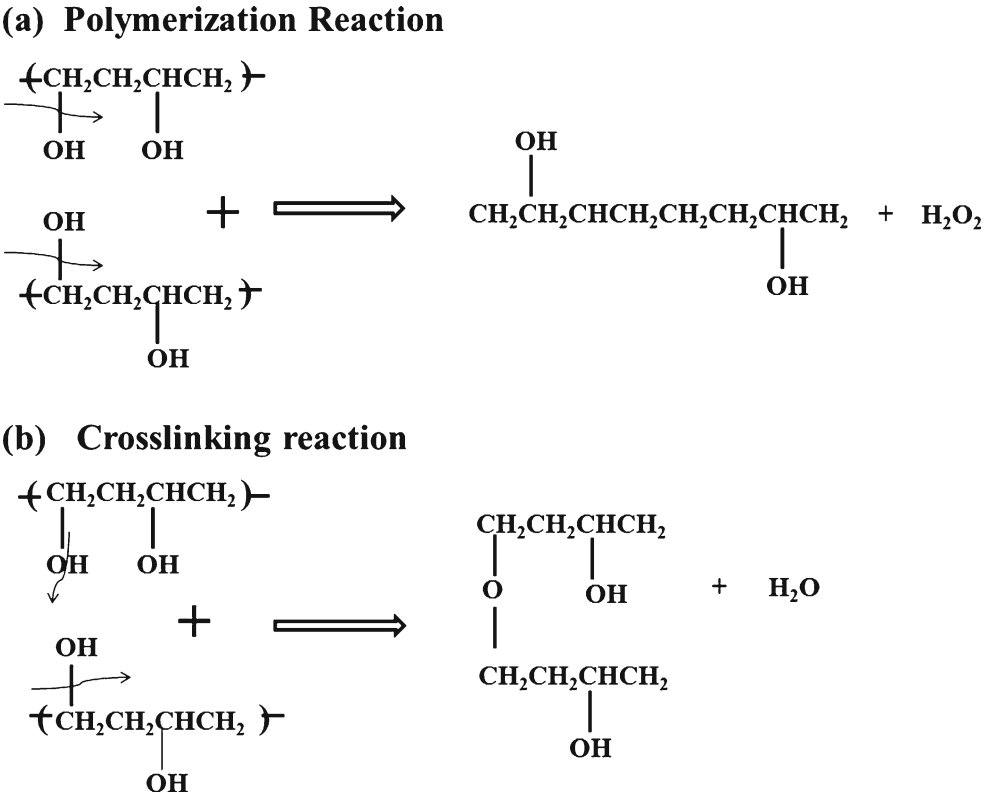

Fig. 5a–b Proposed degradation mechanisms for low and high molecular weight PVAs. **a** Polymerization reaction for PVA-10 k. **b** Crosslinking reaction for PVA-150 k [10]

Computational results

Our experimental results suggested that the thermal degradation of PVA depends on its molecular weight. In order to validate this result and to understand why this should be the case, we carried out ab initio calculations. In the calculations, we assumed that the sample surface is irradiated with X-rays that hit the core electrons of the PVA. We also assumed a correlation between the shift in the experimental core-electron BE when the temperature is increased from 310 to 345 K and the change in the molecular orbital energy of the core electrons when converting from PVA to PVA-5. Figure 6 shows the molecular orbital energies for PVA (blue) and PVA-5 (orange) and the shapes of the molecular orbitals, which are localized on the carbon atoms. When the C–C bond lengths of the PVA are elongated by 5 %, the calculated changes in energy for the molecular orbitals localized at the C–O and C–C bonds are on average 0.22 eV and 0.21 eV (B3PW91/6-31G(d)), respectively. These changes in energy correlated well with the changes that occur in the core-electron binding energy when the sample temperature is increased from 310 to 345 K for PVA-10 k. This suggests that the change in binding energy of 0.2 eV for PVA-10 k is due to thermal stretching. The change in the core BE also suggests that there is a change in the chemical environment of the carbon atoms.

B3PW91 gives more accurate results for chemical properties that mostly depend on core orbitals—for instance, when performing geometric optimizations or when calculating electronic properties of molecular structures [55, 56]—than other functionals such as B3LYP [57] or other methods such

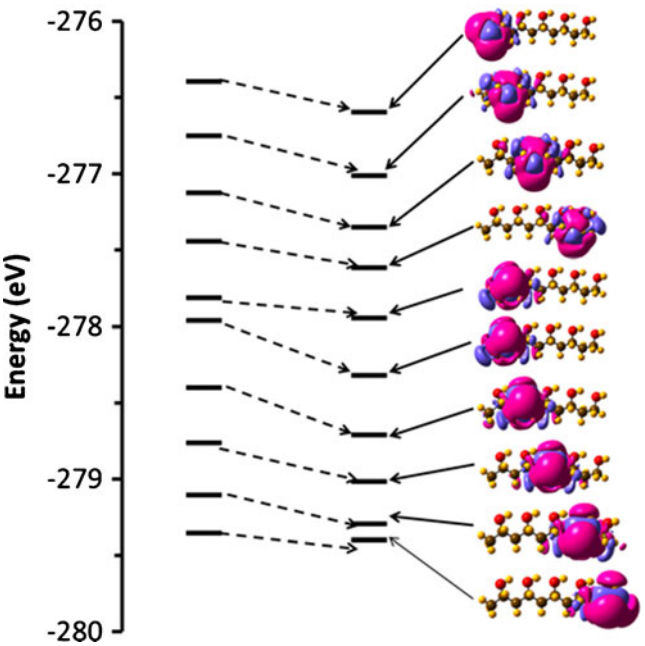

Fig. 6 Molecular orbital energies for the unstretched (*left bars*) and 5 % stretched (*right bars*) C–C bonds of 5-mer polyvinyl alcohol, calculated using the B3PW91/6-31G (d) level of theory. *Orbitals below the red bar* correspond to the 1*s* core electrons from the carbon atoms connected to the OH groups, whereas the *orbitals above the red line* are those from carbon atoms connected only to hydrogen atoms

Table 1 Core energies (eV) of the 1*s* core orbitals of C connected to H atoms only (E_{C-C}) and C connected to OH groups (E_{C-O}) for the unstretched 5-mer polyvinyl alcohol and the 5 % stretched 5-mer polyvinyl alcohol, obtained using several methods and basis sets

Method	Basis set	E_{C-C}	$E_{5\%\ C-C}$	ΔE_{C-C}	E_{C-O}	$E_{5\%\ C-O}$	ΔE_{C-O}
B3PW91	STO-3G	−271.34	−273.40	2.07	−273.44	−271.35	−2.09
B3PW91	STO-6G	−275.15	−275.24	0.10	−277.52	−277.37	−0.16
B3PW91	6-31G(d)	−276.61	−276.81	0.20	−278.22	−278.45	0.23
B3PW91	7-31G(d)	−276.56	−276.75	0.19	−278.17	−278.40	0.23
B3PW91	10-31G(d)	−250.80	−253.07	2.27	−253.02	−250.94	−2.08
B3PW91	12-31G(d)	−276.56	−278.39	1.83	−278.16	−276.75	−1.41
B3PW91	16-31G(d)	−278.17	−278.40	0.23	−276.57	−276.76	0.20
B3PW91	cc-pvDZ	−276.65	−276.85	0.20	−278.19	−278.42	0.23
MP2	6-31G(d)	−307.03			−305.28		
HF	6-31G(d)	−306.91			−305.17		
HF	STO-3G	−301.86			−300.32		
HF	10-31G(d)	−283.84	−283.96	0.12	−281.60	−281.79	0.19
Exp.	XPS	−284.63			−285.63		

as Hartree–Fock (HF). The core-electron energy trends obtained with the B3PW91 functional are acceptable, even though B3PW91 does not calculate the binding energy of the core electrons very accurately. This problem to deal with core electrons is perhaps due to either the basis sets or a systematic problem of the functional. Therefore, we tested STO-3G, STO-6G, and 6-31G(d) as well as the core-uncontracted n-31G(d) (n=7, 10, 12, 16) and cc-pVDZ with the B3PW91 functional. We also used a 10–31(d) uncontracted core where the core exponents were taken from cc-pVDZ, producing a relatively large change in core energies. However, in all of the cases, improving the basis set did not cause any change in the core energies, as shown in Table 1. Therefore, the HF and MP2 approaches were tested using the basis sets 6-31G(d), STO-3G, and 10-31G(d). Acceptable results are obtained for the uncontracted 10-31G basis set using HF.

Table 2 shows how the core energies are affected when the monomer is stretched by 5 %. As the basis set is expanded using the B3PW91 functional, the change in energy of the core orbitals, when stretching the PVA by 5 %, approaches to a limit of 0.23 eV for the unsubstituted carbons and to 0.20 eV for the substituted ones; however, using the HF procedure with the largest basis set, these energy differences become 0.13 and 0.19 eV, respectively. We obtained a good match with DFT for the C–O carbons but not for the CH_2 ones. Perhaps further studies are needed to search for more sophisticated core basis sets.

Table 2 Variations in the core MO energies (in eV) for the C atoms attached to H only (ΔE_{C-C}) and those attached to OH (ΔE_{C-O}) in PVA stretched by 5 %, calculated at several levels of theory

Method	Basis set	ΔE_{C-C}	ΔE_{C-O}
B3PW91	STO-3G	0.07	0.09
B3PW91	STO-6G	0.16	0.14
B3PW91	6-31G(d)	0.23	0.20
B3PW91	7-31G(d)	0.23	0.21
B3PW91	10-31G(d)	0.08	0.14
B3PW91	12-31G(d)	0.23	0.20
B3PW91	16-31G(d)	0.23	0.20
B3PW91	cc-pVDZ	0.23	0.20
HF	10-31G(d)	0.13	0.19

Figure 7 displays $C_{10}H_{19}O_5$, $C_{10}H_{20}O_6$, and $C_{10}H_{22}O_5$ (from the bottom to the top) and the shapes of molecular orbitals (calculated using HF/10-31G (d)) on various functional groups in these species. When the carbonyl group (C=O) and carboxylated group (O–C=O) are added to the PVA, the absolute value for the core energy increases according to the same trend as that observed experimentally (Fig. 7, lines at the bottom). The stretching of PVA with O–C=O functional groups does not yield any changes in the core BE, as shown in Fig. 7 (dashed square).

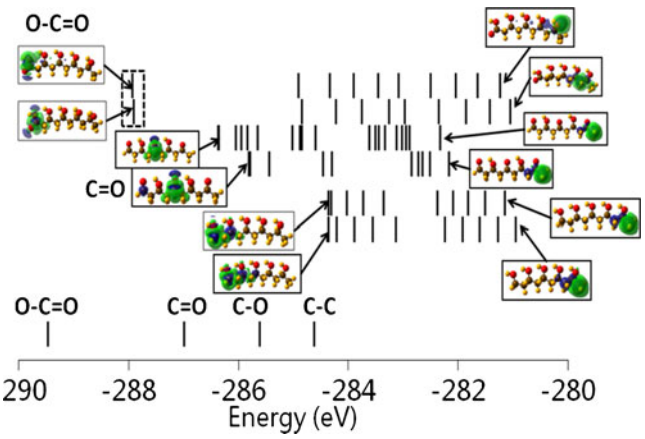

Fig. 7 Molecular orbital energies for PVA and 5 % stretched PVA, calculated using B3PW91 and HF with the 10-31G(d) basis set. Molecular orbital surfaces are plotted with an isovalue of 0.02 au, corresponding to an isodensity of 0.0004 au

Table 3 Total energies (au) for unstretched and 5 % stretched $C_{10}H_{19}O_5$, $C_{10}H_{20}O_6$, and $C_{10}H_{22}O_5$. ΔE (eV) corresponds to the change in the theoretical energy and ΔT (K) to the change in the experimental temperature, as calculated using the expression $\Delta E \approx f\Delta T$. f is a scaling factor used to convert between the theoretical ΔE and the experimental ΔT

Structure	Stoichiometry	E (au)	$E_{5\%}$ (au)	ΔE (eV)	ΔT (K)	f
Fig. 1b	$C_{10}H_{20}O_6$	−756.17349	−756.13927	0.93	0.44	2.12
Fig. 1c	$C_{10}H_{19}O_5$	−750.05417	−750.02093	0.90	0.3	3.02

Table 3 shows the total energies of the unstretched and stretched PVA and the relationship between the change in theoretical total energy and the experimental temperature. There is a proportional factor of ~2.6 when the following definition is used:

$$\Delta E \approx f\,\Delta T,$$

where ΔE corresponds to the change in the theoretical total energy and ΔT to the change in the experimental temperature.

Conclusions

We investigated the effects of mechanothermal forces on the molecular structure of PVA. Standard carbon peaks in PVA were characterized using in situ XPS combined with ab initio calculations. Results showed that under mechanical stretching and thermal expansion, the standard C (1*s*) peaks shift toward higher binding energies. We found that, among all of the functional groups present in PVA, the core electrons in the carbon in C–O groups are the most stable in the temperature range 310–345 K. This is also corroborated by calculations performed at the HF/10–31G(d) level of theory. All binding energies for standard carbon peaks were reproduced with an accuracy of 95 %, thus providing accurate references for future studies of the bonding characteristics and strength of polymers. Finally, the fact that HF yields better results than several of the DFT calculations for the core electrons could be a reason for the major problems with accuracy seen when using present functionals.

Author contributions All authors have given approval to the final version of the manuscript.

Funding sources JMS and DC acknowledge the financial support of the U.S. Defense Threat Reduction Agency (DTRA) through the U.S. Army Research Office, project no. W91NF-06-1-0231, ARO/DURINT project no. W91NF-07-1-0199, and ARO/MURI project no. W911NF-11-1-0024. The ALS is supported by the Director, Office of Science, Office of Basic Energy Sciences, of the U.S. Department of Energy, under contract no. DE-AC02-05CH11231.

References

1. Kar P, Wang K, Liang H (2008) Force-dominated non-equilibrium oxidation kinetics of tantalum. Electrochim Acta 53(16):5084–5091. doi:10.1016/j.electacta.2008.02.034
2. Wang K, Kundu S, Lee H, Liang H (2009) Formation of silver nanochains through mechanoactivation. J Phys Chem C 113(19):8112–8117. doi:10.1021/jp9006087
3. Wang K, Liu Z, Cruz TH, Salmeron M, Liang H (2010) In situ spectroscopic observation of activation and transformation of tantalum suboxides. J Phys Chem A 114(7):2489–2497. doi:10.1021/jp910964s
4. Huitink D, Gao F, Wang K, Liang H (2010) In situ monitoring of tantalum during electrochemical-mechanically induced oxidation. Electrochem Solid-State Lett 13(9):F16–F19
5. Gao F, Liang H (2012) Effects of potential and mechanical stimulation on oxidation of tantalum during electrochemical mechanical polishing. J Electron Mater 41(3):624–631. doi:10.1007/s11664-011-1832-5
6. Gao F, Liang H (2011) Transformable oxidation of tantalum in electrochemical mechanical polishing (ECMP). J Electron Mater 40(2):134–140. doi:10.1007/s11664-010-1443-6
7. Huitink D, Gao F, Liang H (2010) Tribo-electrochemical surface modification of tantalum using in situ AFM techniques. Scanning 32(5):336–344. doi:10.1002/sca.20197
8. Kar P, Wang K, Liang H (2008) Oxidation of tantalum with mechanical force. Electrochem Solid-State Lett 11(2):C13–C17. doi:10.1149/1.2820616
9. Wang K, Rangel NL, Kundu S, Sotelo JC, Tovar RM, Seminario JM, Liang H (2009) Switchable molecular conductivity. J Am Chem Soc 131(30):10447–10451. doi:10.1021/ja901156x
10. Orwoll R (2007) Densities, coefficients of thermal expansion, and compressibilities of amorphous polymers. In: Mark J (ed) Physical properties of polymers handbook. Springer, New York, pp 93–101. doi:10.1007/978-0-387-69002-5_7
11. Lin ZP (1995) Evaluation on two PVA adhesives for gluing transformer insulating components. In: Proc Electrical Electronics Insulation Conf and Electrical Manufacturing & Coil Winding Conf, Rosemont, IL, USA, 18–21 Sept 1995
12. Schlüter K (2000) Textile auxiliaries, 3. sizing agents. In: Ullmann's Encyclopedia of industrial chemistry. Wiley-VCH Verlag GmbH & Co. KGaA. doi:10.1002/14356007.o26_o07
13. Plyusnina AI, Tolmachev IA, Okhrimenko IS (1976) Influences of surfactants (SF) on acid-hydrolysis of polyvinyl acetate (PVA) in aqueous dispersions. J Appl Chem USSR 49(9):2103–2105
14. Mohrova J, Kalinova K (2012) Different structures of PVA nanofibrous membrane for sound absorption application. J Nanomater (in press). doi:10.1155/2012/643043
15. Hassan CM, Peppas NA (2000) Structure and applications of poly(vinyl alcohol) hydrogels produced by conventional crosslinking or by freezing/thawing methods. Adv Polym Sci 153:37–65

16. Kanbara H, Huang SJ, Johnson JF (1994) Measurements of cross-linking degree for electron-beam irradiated block polymers. Polym Eng Sci 34(8):691–694. doi:10.1002/pen.760340811
17. Tomoda Y, Tsuda M (1961) Importance of hydroxyl radicals as intermediates in cross-linking of high polymers by gamma-irradiation. Nature 190(477):905. doi:10.1038/190905a0
18. Tillet G, Boutevin B, Ameduri B (2011) Chemical reactions of polymer crosslinking and post-crosslinking at room and medium temperature. Prog Polym Sci 36(2):191–217. doi:10.1016/j.progpolymsci.2010.08.003
19. Akhter S, Allan K, Buchanan D, Cook JA, Campion A, White JM (1988) XPS and IR study of X-ray-induced degradation of PVA polymer film. Appl Surf Sci 35(2):241–258. doi:10.1016/0169-4332(88)90053-0
20. Beamson G, Briggs D (1998) Degradation of poly(vinyl alcohol) thin films during monochromatized XPS: Substrate effects and X-ray intensity dependence. Surf Interface Anal 26(5):343–351. doi:10.1002/(sici)1096-9918(19980501)26:5<343::aid-sia377>3.0.co;2-m
21. Grass ME, Karlsson PG, Aksoy F, Lundqvist M, Wannberg B, Mun BS, Hussain Z, Liu Z (2010) New ambient pressure photoemission endstation at Advanced Light Source beamline 9.3.2. Rev Sci Instrum 81(5):053106. doi:10.1063/1.3427218
22. Becke AD (1988) Density functional exchange-energy approximation with correct asymptotic behaviour. Phys Rev A 38(6):3098–3100. doi:10.1103/PhysRevA.38.3098
23. Perdew JP, Burke K, Ernzerhof M (1996) Generalized gradient approximation made simple. Phys Rev Lett 77(18):3865–3868. doi:10.1103/PhysRevLett.77.3865
24. Perdew JP, Burke K, Wang Y (1998) Generalized gradient approximation for the exchange-correlation hole of a many-electron system (vol 54, pg 16 533, 1996). Phys Rev B 57(23):14999. doi:10.1103/PhysRevB.57.14999
25. Frisch MJ, Trucks GW, Schlegel HB, Scuseria GE, Robb MA, Cheeseman JR, Scalmani G, BaroneV, Mennucci B, Petersson GA, Nakatsuji H, Caricato M, Li X, Hratchian HP, Izmaylov AF, Bloino J, Zheng G, Sonnenberg JL, Hada M, Ehara M, Toyota K, Fukuda R, Hasegawa J, Ishida M, Nakajima T, Honda Y, Kitao O, Nakai H, Vreven T, Montgomery Jr. JA, Peralta JE, Ogliaro F, Bearpark M, Heyd JJ, Brothers E, Kudin KN, Staroverov VN, Kobayashi R, Normand J, Raghavachari K, Rendell A, Burant JC, Iyengar SS, Tomasi J, Cossi M, Rega N, Millam JM, Klene M, Knox JE, Cross JB, Bakken V, Adamo C, Jaramillo J, Gomperts R, Stratmann RE, Yazyev O, Austin AJ, Cammi R, Pomelli C, Ochterski JW, Martin RL, Morokuma K, Zakrzewski VG, Voth GA, Salvador P, Dannenberg JJ, Dapprich S, Daniels AD, Farkas Ö, Foresman JB, Ortiz JV, Cioslowski J, Fox DJ (2009) Gaussian 09, revision A.02. Gaussian, Inc., Wallingford
26. Collins JB, Schleyer PV, Binkley JS, Pople JA (1976) Self-consistent molecular-orbital methods. 17. Geometries and binding energies of 2nd-row molecules: comparison of 3 basis sets. J Chem Phys 64(12):5142–5151. doi:10.1063/1.432189
27. Dill JD, Pople JA (1975) Self-consistent molecular-orbital method. 15. Extended Gaussian-type basis sets for lithium, beryllium and boron. J Chem Phys 62(7):2921–2923. doi:10.1063/1.430801
28. Seeger R, Pople JA (1976) Self-consistent molecular-orbital methods. 16. Numerically stable direct energy minimization procedures for solution of Hartree–Fock equations. J Chem Phys 65(1):265–271. doi:10.1063/1.432764
29. Petersson GA, Bennett A, Tensfeldt TG, Allaham MA, Shirley WA, Mantzaris J (1988) A complete basis set model chemistry. 1. The total energies of closed-shell atoms and hydrides of the 1st-row elements. J Chem Phys 89(4):2193–2218. doi:10.1063/1.455064
30. Petersson GA, Allaham MA (1991) A complete basis set model chemistry. 2. Open-shell systems and the total energies of the 1st-row atoms. J Chem Phys 94(9):6081–6090. doi:10.1063/1.460447
31. Binkley JS, Pople JA, Hehre WJ (1980) Self-consistent molecular-orbital methods. 21. Small split-valence basis-sets for 1st-row elements. J Am Chem Soc 102(3):939–947. doi:10.1021/ja00523a008
32. Gordon MS, Binkley JS, Pople JA, Pietro WJ, Hehre WJ (1982) Self-consistent molecular-orbital methods. 22. Small split-valence basis-sets for 2nd-row elements. J Am Chem Soc 104(10):2797–2803. doi:10.1021/ja00374a017
33. Pietro WJ, Francl MM, Hehre WJ, Defrees DJ, Pople JA, Binkley JS (1982) Self-consistent molecular-orbital methods. 24. Supplemented small split-valence basis-sets for 2nd-row elements. J Am Chem Soc 104(19):5039–5048. doi:10.1021/ja00383a007
34. Hehre WJ, Ditchfie R, Stewart RF, Pople JA (1970) Self-consistent molecular orbital methods. 4. Use of Gaussian expansions of Slater-type orbitals: extension to second-row molecules. J Chem Phys 52(5):2769. doi:10.1063/1.1673374
35. Newton MD, Lathan WA, Hehre WJ, Pople JA (1970) Self-consistent molecular orbital methods.5. *Ab initio* calculation of equilibrium geometries and quadratic force constants. J Chem Phys 52(8):4064. doi:10.1063/1.1673611
36. Dunning TH (1989) Gaussian basis sets for use in correlated molecular calculations. 1. The atoms boron through neon and hydrogen. J Chem Phys 90(2):1007–1023. doi:10.1063/1.456153
37. Seminario JM, Concha MC, Politzer P (1992) Calculated structures and relative stabilities of furoxan, some 1,2-dinitrosoethylenes and other isomers. J Comput Chem 13(2):177–182
38. Politzer P, Seminario JM (1993) Energy changes associated with some decomposition steps of 1,3,3-trinitroazetidine: a nonlocal density-functional study. Chem Phys Lett 207(1):27–30
39. Seminario JM, Derosa PA, Cordova LE, Bozard BH (2004) A molecular device operating at terahertz frequencies. IEEE Trans Nanotechnol 3(1):215–218
40. Politzer P, Seminario JM (1993) Computational study of the structure of dinitraminic acid, $HN(NO_2)_2$ and the energetics of some possible decomposition steps. Chem Phys Lett 216:348–352
41. Murray J, Redfern P, Seminario J, Politzer P (1990) Anomalous energy effects in some aliphatic and alicyclic aza systems and their nitro-derivatives. J Phys Chem 94(6):2320–2323
42. Seminario JM, Tour JM (1997) Systematic study of the lowest energy states of Au_n (n=1–4) using DFT. Int J Quantum Chem 65:749–758
43. Seminario JM, Agapito LA, Yan L, Balbuena PB (2005) Density functional theory study of adsorption of OOH on Pt-based bimetallic clusters alloyed with Cr, Co, and Ni. Chem Phys Lett 410(4–6):275–281
44. Seminario JM, Zacarias AG, Castro M (1997) Systematic study of the lowest energy states of Pd, Pd_2, and Pd_3. Int J Quantum Chem 61:515–523
45. Murray JS, Seminario JM, Politzer P (1994) Does antiaromaticity imply net destabilization. Int J Quantum Chem 49(5):575–579
46. Rangel NL, Sotelo JC, Seminario JM (2009) Mechanism of carbon-nanotubes unzipping into graphene ribbons. J Chem Phys 131(031105):031101–031104
47. Seminario JM, Ma Y, Agapito LA, Yan L, Araujo RA, Bingi S, Vadlamani NS, Chagarlamudi K, Sudarshan TS, Myrick ML, Colavita PE, Franzon PD, Nackashi DP, Cheng L, Yao Y, Tour JM (2004) Clustering effects on discontinuous gold film nanocells. J Nanosci Nanotechnol 4(7):907–917

48. Balbuena PB, Calvo SR, Lamas EJ, Salazar PF, Seminario JM (2006) Adsorption and dissociation of H_2O_2 on Pt and Pt-alloy clusters and surfaces. J Phys Chem B 110:17452–17459
49. Seminario JM, Concha MC, Murray JS, Politzer P (1994) Theoretical analyses of O_2/H_2O systems under normal and supercritical conditions. Chem Phys Lett 222(1–2):25–32
50. Sotelo JC, Yan L, Wang M, Seminario JM (2007) Field induced conformational changes in bimetallic oligoaniline junctions. Phys Rev A 75(2):022511 (022513 pages)
51. Seminario JM (1996) Calculation of intramolecular force fields from second-derivative tensors. Int J Quantum Chem 60(7):1271–1277
52. Akhter S, Jo S, Zhou XL, White J (1989) XPS identification of Al-PVA complex. MRS Proc 153:157. doi: 10.1557/PROC-154-241
53. Samir F, Benseddik E, Corraze B, Bernede C, Morsli M, Bonnet A, Conan A, Lefrant S (1995) XPS and transport studies of PVA-PPY and PST-PBTH composites. Synth Met 69(1–3):341–342. doi:10.1016/0379-6779(94)02476-f
54. Scholes PD, Coombes AGA, Illum L, Davis SS, Watts JF, Ustariz C, Vert M, Davies MC (1999) Detection and determination of surface levels of poloxamer and PVA surfactant on biodegradable nanospheres using SSIMS and XPS. J Control Release 59(3):261–278. doi:10.1016/s0168-3659(98)00138-2
55. Xiao H, Tahir-Kheli J, Goddard WA III (2011) Accurate band gaps for semiconductors from density functional theory. J Phys Chem Lett 2(3):212–217. doi:10.1021/jz101565j
56. Perez-Angel EC, Seminario JM (2011) *Ab initio* analysis and harmonic force fields of gallium nitride nanoclusters. J Phys Chem C 115(14):6467–6477. doi:10.1021/jp201004w
57. Graciani J, Marquez AM, Plata JJ, Ortega Y, Hernandez NC, Meyer A, Zicovich-Wilson CM, Sanz JF (2011) Comparative study on the performance of hybrid DFT functionals in highly correlated oxides: the case of CeO_2 and Ce_2O_3. J Chem Theory Comput 7(1):56–65. doi:10.1021/ct100430q